Adaptive PID Control for Autopilot Design of Small Fixed Wing UAVs

Tanzil Ahmed Lohani[1], *Abhishek* Dixit[1] and *Pooja* Agrawal[2*]

[1]Department of Aerospace Engineering, Defence Institute of Advanced Technology (DIAT), DU, Pune, India
[2]Assistant Professor, School of Robotics, Defence Institute of Advanced Technology (DIAT), DU, Pune, India

Abstract. The development of a flight control system for the class of small fixed wing Unmanned Aerial Vehicle (UAV) imposes a challenge to the designers to achieve acceptable and stable performance characteristics across the defined flight envelope. This paper focuses on developing a dynamic model of the Aerosonde UAV, incorporating it with an adaptive Proportional, Integral and Derivative (PID) control system for designing both lateral and longitudinal autopilots. The PID gains for each control loop are self-tuned based on an analytical approach, making sure that the desired command value is achieved at each time interval as closely as possible. To check the robust nature of the designed control system in the presence of external wind disturbance, a Dryden wind gust model was developed, and the entire simulation results were carried out in MATLAB®/Simulink environment. The proposed adaptive PID controller proves the effectiveness and robustness of the autopilot control system.

1 Introduction

In the past few decades, Unmanned Aerial Vehicles (UAVs) have gained interest and importance in both the defence and civilian fields. And this is majorly because of their characteristics like accessibility, low cost and no human-life risk involvement. UAVs have predominantly proved their success in high-risk missions ranging from search and rescue operations carried out during natural disasters like earthquakes and floods, in national defence, weather monitoring and so on. In all such scenarios, the presence of a human being in flight was never imagined [1-3]. The execution of a successful UAV flight depends greatly on its autonomous controller termed autopilot. An autopilot's job is to control UAVs flight by continuously tracking the desired flight path accurately and to make sure its design is robust in regard to adverse environmental conditions involving wind gusts. Apart from path tracking autopilot controls the aircraft's attitude, airspeed and altitude [4]. In cases of small UAVs the wind velocity magnitude greatly effects its performance since it matches closely with the actual UAVs speed. As a result of which engineers face a greater

* Corresponding author: poojaa.diat@gmail.com

challenge in designing an efficient autopilot system for UAVs. In recent era usage of modern control theory for designing control system algorithms for UAV autopilots have been successfully established, but these are majorly based on nonlinear control, new and progressive algorithms. Even though such autopilots have shown their success, only a few reports are documented. Due to their complexity, nonlinear behaviour and high computational cost there is less interest in engineers to employ them in physical UAV autopilot systems. An alternative option would be PID (Proportional, Integral and Derivative) autopilots, which are integrated in real-time control systems. Because PID autopilots have a simple structure, easy to implement without sacrificing on acceptable performance characteristics defined for the UAV autopilot. However, PID autopilots need a proper understanding of the mathematical model of the aircraft under consideration and tuning methods to achieve improved performance over the entire flight envelope [5].

The fixed wing UAVs configuration is closely related to the conventional aircraft design for manned operations. The dynamic model of fixed wing UAVs is immensely characterized to be nonlinear and highly coupled. External disturbance like wind gust affects the dynamic model for such an aircraft [4].

This paper aims to design an adaptive PID controller for a fixed wing Aerosonde UAV [6], that has the capability of controlling the aircraft's longitudinal and lateral motion. The controller design process requires firstly a thorough modelling of the Aerosonde aircraft based on kinematics and dynamics equations for rigid-body derived from Newton's second law of motion. The aerodynamic forces (lift and drag) and the aircraft inertia are taken into consideration. The MATLAB®/Simulink environment is used to execute the dynamic model for Aerosonde UAV. Then trimming the Aerosonde dynamic model based on optimization through penalty method is carried out. Next, the adaptive PID based autopilots are developed for longitudinal (pitch and altitude hold) and lateral (roll and yaw attitude hold) cases. The gains of PID control loops are tuned with an analytical method. To check the robust nature of the developed PID controller in the presence of wind disturbance, a Dryden wind gust model is considered.

2 The Aerosonde UAV description and dynamic model

2.1 Aircraft description

The Aerosonde is a small, autonomous, fixed wing UAV designed mainly for weather surveillance. Aerosonde was the first UAV to cross the Atlantic Ocean in 1998. Figure 1, [7] shows the aerosonde UAV model. The general specifications of the UAV are listed in Table 1 [8]. Even though Aerosonde is equipped with a complicated control system, it has high flexibility in its design that makes it suitable to command the aircraft effectively from any location [9].

Fig. 1. Aerosonde UAV model [7].

Table 1. Aerosonde UAV specifications.

Specifications	
Mass (m)	13.5 kg
Wing span (b)	2.8956 m
Flight	Fully autonomous
Maximum speed	30-40 m/s
Cruise speed	20-30 m/s
Operational altitude range	~6096 m
Payload	1 kg
Wing chord (c)	0.19 m

2.2 Aerosonde UAV dynamic model

In order to build the 6-DoF UAV model for the aircraft, the UAV is assumed to be a rigid-body, with the entire mass being symmetrically distributed about the aircraft's absolute coordinate system [10], this is based on a non-linear model described by Newton's second law and is represented by 12 dynamic state variables listed in Table 2 using 12 dynamic equations [11].

Table 2. State variables for UAV equations of motion.

Symbol	Description
P_n	Inertial north position of UAV along $\mathbf{i}^{\mathbf{i}}$ axis of inertial frame
P_e	Inertial east position of the UAV along $\mathbf{j}^{\mathbf{i}}$ axis of inertial frame
P_d	Inertial down position (negative of altitude) of the UAV along $\mathbf{k}^{\mathbf{i}}$ axis of inertial frame
u	Body frame velocity measured along $\mathbf{i}^{\mathbf{b}}$ axis of body frame
v	Body frame velocity measured along $\mathbf{j}^{\mathbf{b}}$ axis of body frame
w	Body frame velocity measured along $\mathbf{k}^{\mathbf{b}}$ axis of body frame
p	Roll rate measured along $\mathbf{i}^{\mathbf{b}}$ axis of body frame
q	Pitch rate measured along $\mathbf{j}^{\mathbf{b}}$ axis of body frame
r	Yaw rate measured along $\mathbf{k}^{\mathbf{b}}$ axis of body frame
ϕ	Roll angle defined with respect to vehicle frame
θ	Pitch angle defined with respect to vehicle frame
ψ	Yaw angle defined with respect to vehicle frame

Where $\mathbf{i}^{\mathbf{b}}$, $\mathbf{j}^{\mathbf{b}}$ and $\mathbf{k}^{\mathbf{b}}$ are axes that run from the centre of gravity point of the UAV towards the nose, right wing and vertically down respectively. Hence the state variables of UAV are represented in vector form as

$$\mathrm{X} = (u, v, w, p, q, r, \phi, \theta, \psi, P_n, P_e, P_d) \tag{1}$$

All the propeller properties, aerodynamic coefficients and moments of inertia values for the aerosonde aircraft which is to be dynamically modelled are required to be substituted in the 12 dynamic equations which are as follows;

Force equation

$$\begin{pmatrix} \dot{u} \\ \dot{v} \\ \dot{w} \end{pmatrix} = \frac{1}{m}\begin{pmatrix} f_x \\ f_y \\ f_z \end{pmatrix} + \begin{pmatrix} vr - qw \\ pw - ur \\ qu - pv \end{pmatrix} \tag{2) (3) (4}$$

Moment equation

$$\begin{pmatrix}\dot{p}\\ \dot{q}\\ \dot{r}\end{pmatrix} = \begin{pmatrix}\mathbb{\Gamma}_1 pq - \mathbb{\Gamma}_2 qr + \mathbb{\Gamma}_3 l + \mathbb{\Gamma}_4 n\\ \mathbb{\Gamma}_5 pr - \mathbb{\Gamma}_6 (p^2 - r^2) + \frac{m_m}{I_y}\\ \mathbb{\Gamma}_7 pq - \mathbb{\Gamma}_1 qr + \mathbb{\Gamma}_4 l + \mathbb{\Gamma}_8 n\end{pmatrix} \quad (5)\ (6)\ (7)$$

Kinematic equation

$$\begin{pmatrix}\dot{\phi}\\ \dot{\theta}\\ \dot{\psi}\end{pmatrix} = \begin{pmatrix}p + qtan(\theta)s(\phi) + rtan(\theta)c(\phi)\\ qc(\phi) - rs(\theta)\\ q\frac{s(\phi)}{c(\theta)} + r\frac{c(\phi)}{c(\theta)}\end{pmatrix} \quad (8)\ (9)\ (10)$$

Navigation equation

$$\begin{pmatrix}\dot{P}_n\\ \dot{P}_e\\ \dot{P}_d\end{pmatrix} = \begin{pmatrix}u(c(\theta)c(\psi)) + v(s(\phi)s(\theta)c(\psi) - c(\phi)s(\psi)) + w(c(\phi)s(\theta)c(\psi) + s(\phi)s(\psi))\\ u(c(\theta)s(\psi)) + v(s(\phi)s(\theta)s(\psi) + c(\phi)c(\psi)) + w(c(\phi)s(\theta)s(\psi) - s(\phi)c(\psi))\\ -u(s(\theta)) + vs(\phi)c(\theta) + wc(\phi)c(\theta)\end{pmatrix} \quad (11)(12)(13)$$

Where f_x, f_y and f_z represent the x, y and z components of forces acting on UAV in the body frame respectively. Similarly, the x, y and z (roll, pitch and yaw) components of torque (moment) acting on UAV in the body frame is represented by l, m_m and n respectively. Here s and c denote the sine and cosine of corresponding angles. $\mathbb{\Gamma}_1$ to $\mathbb{\Gamma}_8$ represent inertial parameters.

A dynamic model is then created for the aerosonde UAV in the Simulink workspace. Which is a non-linear 6-DoF plant model. The Figure 2 represents the generic block diagram representation of the dynamic model along with the PID controller connected with it. The control vector U is defined as given in Equation (14).

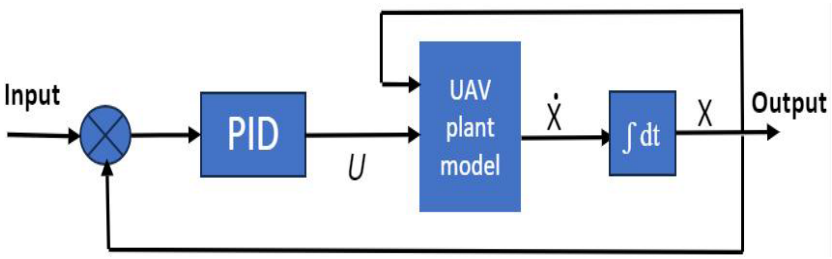

Fig. 2. Dynamic model.

$$U = (\delta_a, \delta_e, \delta_r, \delta_t)^{\mathrm{T}} \quad (14)$$

Here $\delta_a, \delta_e, \delta_r,$ and δ_t represent aileron, elevator, rudder deflections and throttle command respectively.

Thereafter the non-linear 6-DoF plant model is trimmed for steady state and level flight (SSLF) conditions at 50 meters initial altitude. Optimization through Penalty method is used to trim the model [12]. The objective function was to minimize $\dot{X}$ subject to the constraints of SSLF which include Va (airspeed) to be fixed at a constant value of 25 m/s, flight path angle γ, roll angle ϕ, yaw angle ψ and y component of velocity v such that all will achieve zero state. In order to convert from constrained to unconstrained optimization problem penalty method comes in handy, where the objective function $F_0(Q)$ as given by

Equation (15) is now modified to include the SSLF constraints defined earlier along with $\dot{X}$. Here, *fminsearch* function defined in MATLAB is used to find the global minimum of the updated cost function. The optimization process is terminated once all constraints are met and the objective function is zero. The optimization process yielded the trim states X^* and corresponding trim control vectors U^* which are described through Equations (16) and (17).

$$F_0(Q) = Q^{\mathrm{T}} \times H \times Q \tag{15}$$

Where $Q = (\dot{X}, \mathrm{Va}-25, \gamma, \phi, \psi, v)^{\mathrm{T}}$

H = A diagonal matrix of penalty parameters α.

$$X^* = \begin{pmatrix} u^* \\ v^* \\ w^* \\ p^* \\ q^* \\ r^* \\ \phi^* \\ \theta^* \\ \psi^* \end{pmatrix} = \begin{pmatrix} 24.9153 \\ -6.1623e^{-12} \\ 2.0557 \\ -7.8974e^{-12} \\ -5.9597e^{-12} \\ -3.7812e^{-12} \\ -9.9756e^{-12} \\ 0.0823 \\ -1.04e^{-11} \end{pmatrix} \tag{16}$$

$$U^* = \begin{pmatrix} {\delta_a}^* \\ {\delta_e}^* \\ {\delta_r}^* \\ {\delta_t}^* \end{pmatrix} = \begin{pmatrix} -5.0563e^{-13} \\ -0.1093 \\ -8.9993e^{-13} \\ 0.3335 \end{pmatrix} \tag{17}$$

The trimmed non-linear plant model of the UAV is now linearized about this trim point using the linear analysis tool of Simulink. The model is also equipped with a saturation check for the control surface deflection limitations [13]. To validate the SSLF condition the U^* and X^* values are fed into the model as initial conditions and the simulation is executed for 15 seconds time period and the results are shown in Figure 3, the plots prove that the aircraft model maintains itself in the steady state throughout the simulation period.

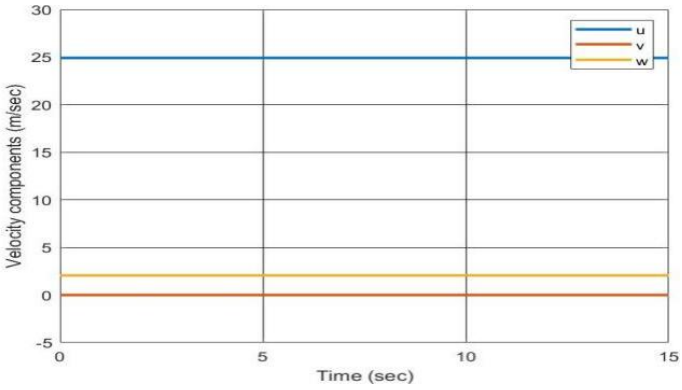

(a) Velocity components

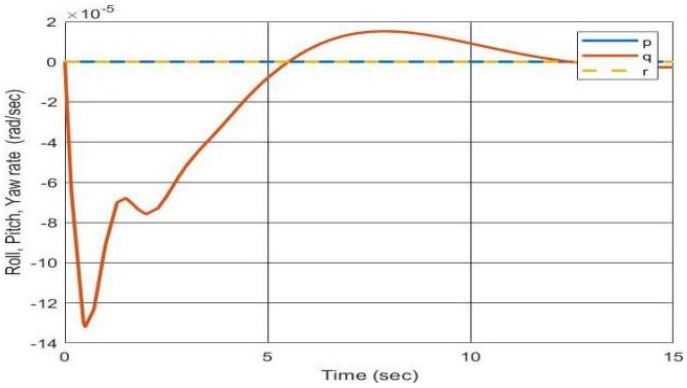

(b) Angular rates

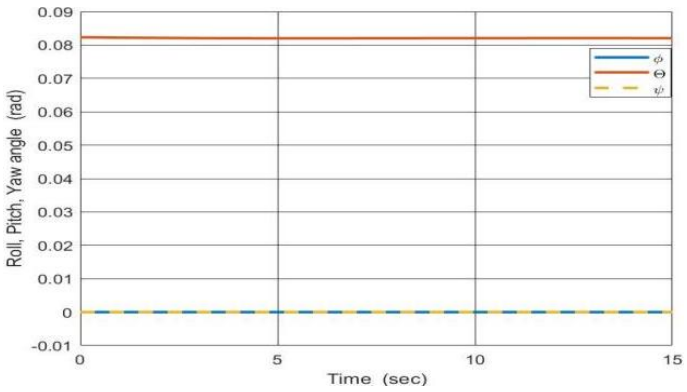

(c) Euler angles

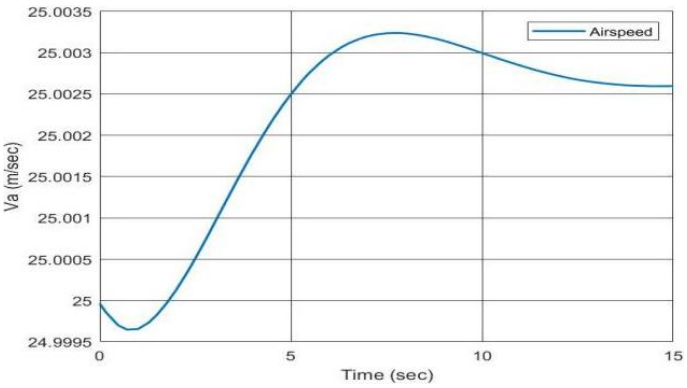

(d) Airspeed

Fig. 3. Trim validation.

3 Controller design

The success of any UAV flight depends on how reliable is the control system designed for carrying out the desired mission. The PID controller is the most widely used and proven controller for UAVs, the fact that PID controllers can easily be implemented in any aircraft system substantiates their extensive usage in today's world of controllers. The UAV control

system is bifurcated into two controllers. The primary controller being the "Lateral Controller" and the other "Longitudinal Controller" [14]. The job of the lateral controller is to control the roll angle and heading (yaw) angle of the UAV. The pitch angle, altitude and airspeed are regulated by the lateral controller. Any controller designed achieves the desired performance characteristics of the UAV by continuously reducing the error term (difference between current state and desired state), hence a closed loop control system is necessary [15].

Proportional, Integral and Derivative terms make up a PID controller. The transfer function of the PID controller is given as

$$\mathrm{H(s)} = \frac{K_d.S^2+K_p.S+K_I}{S} \tag{18}$$

Where K_p, K_d and K_I represent proportional, derivative and integral gain constants. In real time PID controllers perform in the presence of external disturbance. Thus often for researchers and engineers, it's a great challenge to appropriately tune the gain constants of the PID controller in the above mentioned situation. In [13], the following techniques for tuning a PID controller are discussed,

- Trial and error method
- Analytical method
- Empirical method

In this work, the PID controller gains are adaptive and their formulation is based on formula based analytical method described in [11].

3.1 Autopilot design

In this work, the successive loop closure technique is utilized to design both lateral and longitudinal autopilot systems for aerosonde UAV [11]. In designing the autopilot with the mentioned technique, an assumption that the longitudinal dynamics are decoupled from the lateral dynamics is considered. This paper aims to design an adaptive PID based lateral autopilot system for controlling roll and yaw commands, similarly a longitudinal autopilot system for controlling pitch and altitude commands. The basic idea behind the successive loop closure technique is to wrap several simple feedback loops in succession around the plant dynamic model created. An important condition for this technique to be implemented is that the inner loop must have a higher bandwidth than the outer loop. Usually, the bandwidth separation between the loops is a factor of around 5 to 10.

3.1.1 Lateral autopilot design

For the lateral autopilot system, the inner loop is the roll attitude hold loop which is used to control roll angle ϕ and roll rate p. The outer loop is used for directional control (yaw angle ψ) of the UAV. The generic block diagram for such a lateral control loop is shown in Figure 4 (a).

The outer PID loop for directional control takes in the commanded yaw angle (ψ^c) as input and an error value is developed between this ψ^c and the current ψ state that is fed back from the plant. Thereafter appropriate PID gain values are obtained by analytical formulas given in [11], which also depend on the current airspeed (V_a). The output of this outer yaw PID loop is ϕ^c (roll command) state.

The inner PID loop for roll control takes in this ϕ^c state as input, this is then added to the ϕ^c actually commanded by the user and an error value is developed between the total ϕ^c and current ϕ state that is fed back from the plant. As mentioned above, the appropriate

adaptive PID gain values are obtained by analytical formulas [11]. This inner PID loop has δ_a as output which is fed into the UAV dynamic plant model.

The complete lateral autopilot is modelled in Simulink workspace and connected to plant dynamics. With regard to the yaw control lateral autopilot, a PI controller is developed and for roll control lateral autopilot, a PD controller is developed.

3.1.2 Longitudinal autopilot design

In the case of the longitudinal autopilot system, the inner loop is the pitch attitude hold loop which is used to control pitch angle θ and pitch rate q. The outer altitude hold loop is used to achieve the desired altitude value for the UAV. The generic block diagram for such a longitudinal control loop is shown in Figure 4 (b).

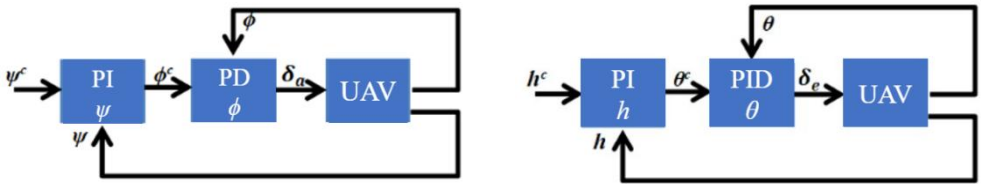

(a) Lateral (b) Longitudinal

Fig. 4. Autopilot system.

The outer PID loop for altitude control takes in the commanded altitude h^c as input. And an error value is developed between h^c and the current altitude h state that is fed back from the plant. The appropriate PID gain values are obtained by analytical formulas given in [11]. The output of this outer altitude PID loop is θ^c (pitch command) state.

The inner PID loop for pitch attitude control takes in this θ^c state as input, along with the θ^c actually commanded by the user and an error value is developed between this θ^c and the current θ state which is fed back from the plant. Then appropriate PID gain values are obtained by analytical formulas as given in [11]. This inner PID loop has δ_e as output which is fed into the UAV dynamic plant model.

Here the altitude control autopilot is based on an adaptive PI controller and for pitch attitude control autopilot an adaptive gain based PID controller is developed.

4 Dryden wind gust model

To check the effectiveness of the proposed adaptive gain based PID control system developed and to analyze the dynamic response of the UAV to external disturbances, the Dryden wind gust model is used in this work. The turbulence intensity σ and spatial wavelengths L are two parameters of the Dryden wind gust model. The Dryden transfer functions defined in [11] are used to build the model. A nominal constant airspeed of 15m/s is assumed for the implementation of Dryden model. The MIL-F-8785C military specification defines the values of these parameters at different altitudes. Suitable parameters for low and medium altitudes with light and moderate turbulence levels are presented in [16] and are shown in Table 3. The plant model is now updated to have additional inputs from the gust model developed.

Table 3. Dryden wind gust parameters.

Gust description	Altitude h (m)	$L_u = L_v$ (m)	L_w (m)	$\sigma_u = \sigma_v$ (m/s)	σ_w (m/s)
Low altitude, light turbulence	50	200	50	1.06	0.7
Low altitude, moderate turbulence	50	200	50	2.12	1.4
Medium altitude, light turbulence	600	533	533	1.5	1.5
Medium altitude, moderate turbulence	600	533	533	3	3

5 Simulation results

The developed autopilots are assessed in the presence of external wind conditions. The roll, yaw, pitch and altitude control loops are given a triangular input command and the corresponding response obtained from the plant is studied. The medium altitude, moderate turbulence class of the Dryden wind gust model is chosen to demonstrate the robustness of the developed adaptive PID autopilot system. The UAV is maintained at the trim condition at zero time instant (initial condition) and at an altitude of 600 meters.

5.1 Lateral autopilot

Figure 5 (a) shows the triangular input response of roll only adaptive control loop. It is observed that the response of ϕ is closely matched with ϕ^c. Figure 5 (b) displays the corresponding $K_d\phi$ and $K_p\phi$ gain variation.

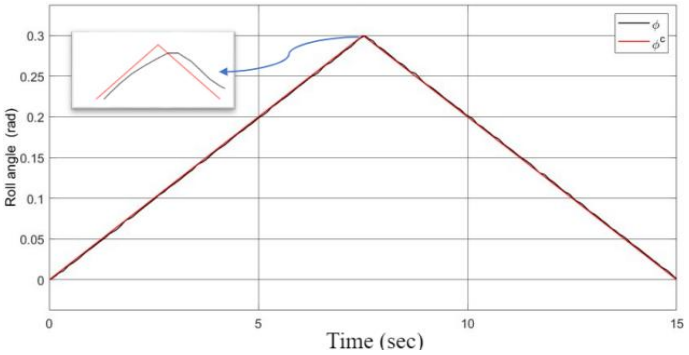

(a) Roll triangular response

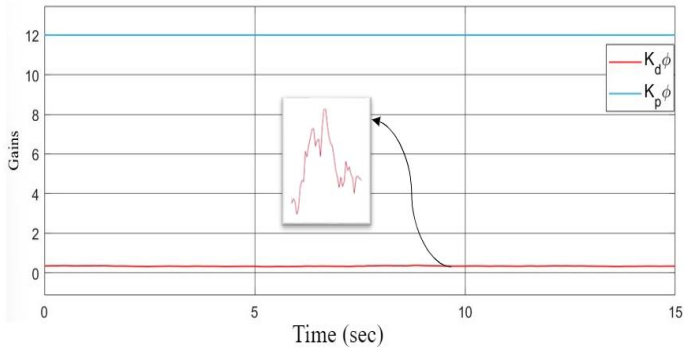

(b) Gain variation

Fig. 5. Roll only adaptive PID.

Figure 6 (a) presents the triangular input response for yaw and roll (complete lateral autopilot) adaptive control loop. It is seen that the response of ψ is closely following ψ^c. Corresponding $K_I\psi$ and $K_p\psi$ gain variations can be observed in Figure 6 (b). The ϕ commanded due to this yaw loop and the roll initially commanded in triangular form earlier (Fig 5), collectively gives the total ϕ^c, Figure 6 (c) depicts the response of the total ϕ^c achieved from the lateral adaptive PID control loop. The corresponding $K_d\phi$ and $K_p\phi$ gain variation is captured in Figure 6 (d).

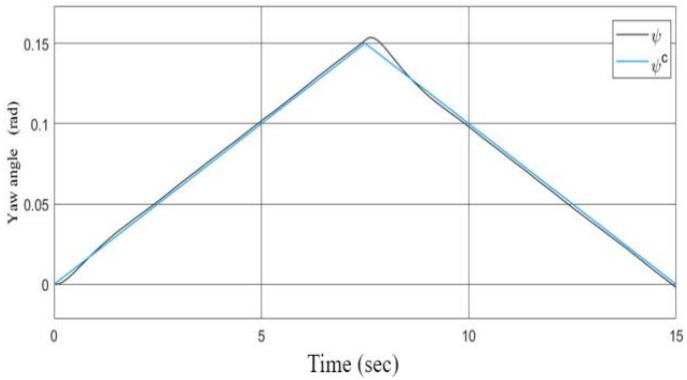

(a) Yaw triangular response

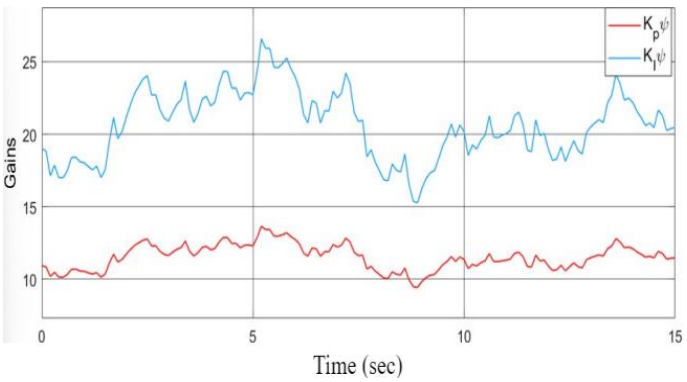

(b) Gain variation

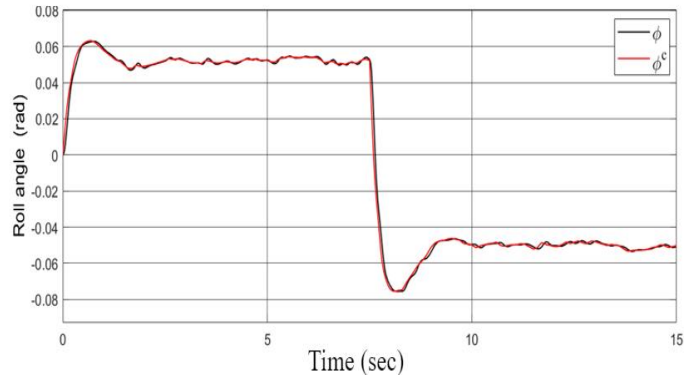

(c) Roll response

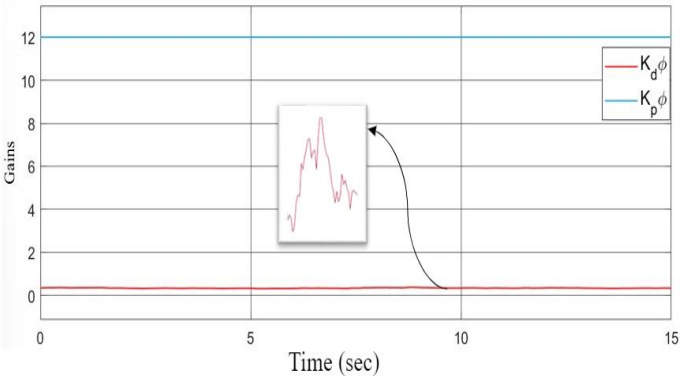

(d) Gain variation

Fig. 6. Complete lateral adaptive PID.

5.2 Longitudinal autopilot

The Pitch only adaptive control loop performance for applied triangular input is displayed through Figure 7 (a). It is observed that the response of θ is closely matched with θ^c. The variation of $K_p\theta$, $K_I\theta$ and $K_d\theta$ gains is visible in Figure 7 (b).

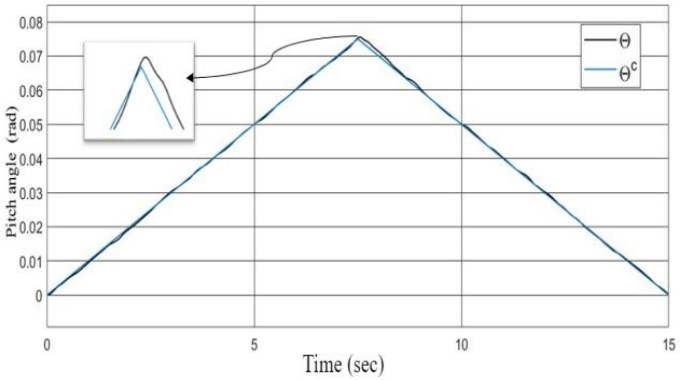

(a) Pitch triangular response

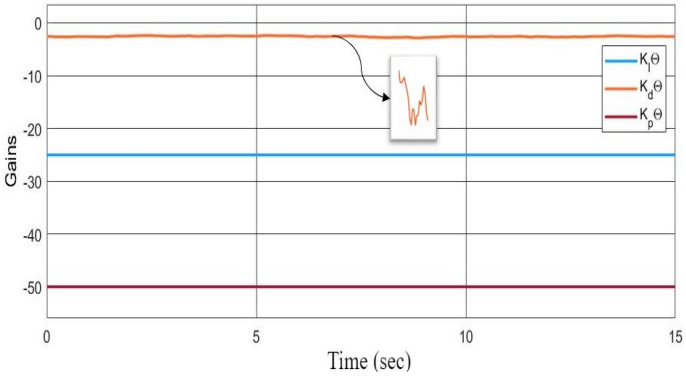

(b) Gain variation

Fig. 7. Pitch only adaptive PID.

At this point, Figure 8 (a) deals with the triangular input response for altitude and pitch (complete longitudinal autopilot) adaptive control loop. It is observed that the response of h is closely tracking h^c. Figure 8 (b) shows the corresponding gains $K_p h$ and $K_I h$ variation. The change in θ commanded due to this altitude loop and the change in pitch initially commanded in triangular form earlier (Fig 7), collectively provide the total θ^c. Figure 8 (c) shows the response of total θ^c achieved from the longitudinal adaptive PID control loop. Figure 8 (d) depicts the corresponding gains $K_p\theta$, $K_I\theta$ and $K_d\theta$ variation.

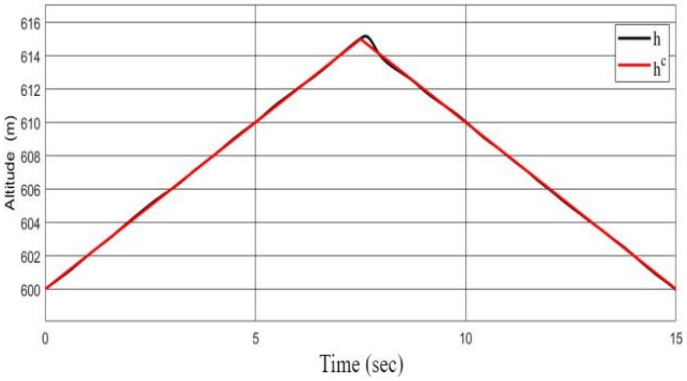

(a) Altitude triangular response

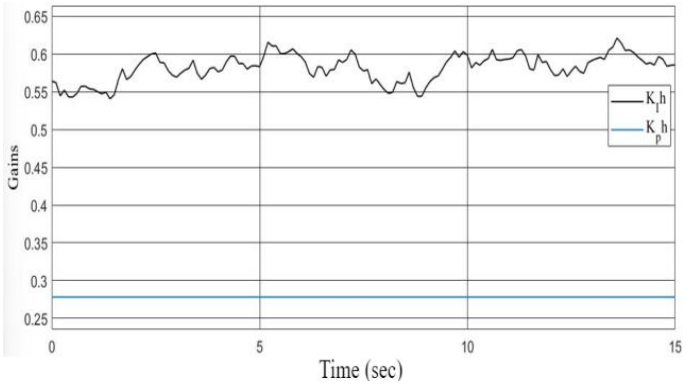

(b) Gain variation

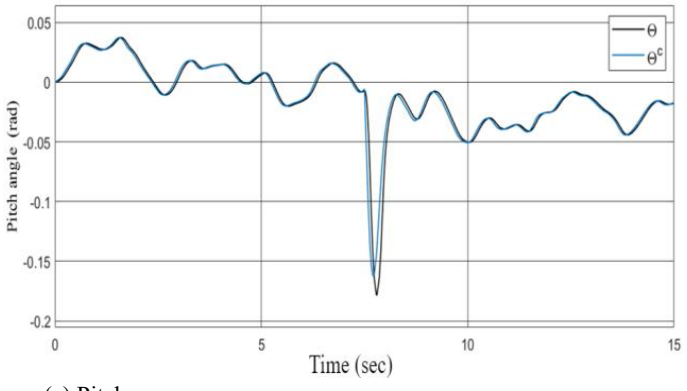

(c) Pitch response

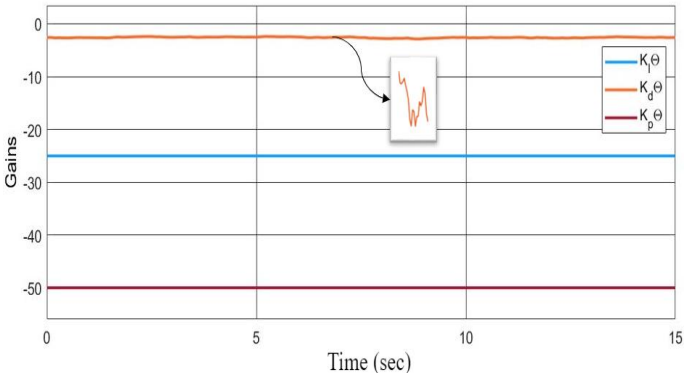

(d) Gain variation

Fig. 8. Complete longitudinal adaptive PID.

6 Conclusion

A Dynamic model of the Aerosonde UAV was developed and the adaptive PID autopilot controller was proposed for controlling both the attitude and altitude of the aircraft, the self-tuning based on adaptive PID gains was possible with the help of an analytical approach. The proposed controller was simulated under the existence of external wind disturbance. The external wind disturbance is based on the Dryden wind gust model. The results successfully validate the robustness of the autopilot system by effectively handling moderate turbulence at medium altitude.

References

1. J. Xu, Q. Guo, L. Xiao, Z. Li, G. Zhang, Autonomous Decision-Making Method for Combat Mission of UAV based on Deep Reinforcement Learning, in 4th (IAEAC) conference, 538-544 (2019)
2. Y. Sato, T. Yamasaki, H. Takano, Y.Baba, Trajectory Guidance and Control for a Small UAV, Int. J. Aeronaut. Space Sci. **7**, 137-144 (2006)
3. Valavanis, P. Kimon, Advances in Unmanned Aerial Vehicles (ISCA, Volume 33) Design and Control of a Miniature Quadrotor, (Springer 2007)
4. H. Castaneda, J. Morales, E. Diaz, Quasi-Continuous Sliding Mode Flight Control for a Fixed-Wing UAV, Congreso Nacional de Control Automatico, Ensenada, Baja California, Mexico, (October 2013)
5. B. Kada, Y. Ghazzawi, Robust PID Controller Design for an UAV Flight Control System, World Congress on Engineering, (2011)
6. https://www.textronsystems.com/products/aerosonde-uas, as visited on 17-November-2023
7. https://commons.wikimedia.org/wiki/Aerosonde, as visited on 17-November-2023
8. M. Niculescu, Lateral Track Control Law for Aerosonde UAV. 39th AIAA conference, USA (2001)
9. A. Sarhan, S. Qin, Robust Adaptive Flight Controller for UAV Systems, 4th ICISCE conference, 1214-1219 (2017)

10. B.Zhu, J. Zhu, Q. Chen, A bio-inspired flight control strategy for a tail-sitter unmanned aerial vehicle, Sci. China Inf. Sci. **63**, 1-10 (2020)
11. R. Beard, T. McLain, Small Unmanned Aircraft: Theory and Practice, (Princeton University Press, Princeton 2012)
12. O. Yeniay, Penalty Function Methods for Constrained Optimization with Genetic Algorithms. Math. Comput. Appl. **10**, 45-56 (2005)
13. A. Elbatal, A. Youssef, M. Elkhatib, Smart aerosonde UAV longitudinal flight control system based on genetic algorithm, Bul. Elect. Eng. Info. 2433-2441 (2021)
14. F.Lin, H. Duan, X. Qu, PID control strategy for UAV flight control system based on improved genetic algorithm optimization, 26th CCDC conference, 92-97 (2014)
15. S. Mathisen, F. Leira, H. Helgesen, K.Gryte, T. Johansen, Autonomous ballistic airdrop of objects from a small fixed-wing unmanned aerial vehicle, Auton. Robots, **44**, 859-875 (2020)
16. J. Langelaan, N. Alley, J. Neidhoefer, Wind Field Estimation for Small Unmanned Aerial Vehicles, J. Guid. Control Dyn. **34**, 1016-1030 (2010)